Exact lens equation for the Einstein-Euler-Heisenberg static black hole

Daniel Amaro[*]

Departamento de Física, Universidad Autónoma Metropolitana–Iztapalapa,
PO. Box 55–534, C.P. 09340, Ciudad de México, México

Alfredo Macías[†]

Physics Department, Universidad Autónoma Metropolitana–Iztapalapa,
PO. Box 55–534, C.P. 09340, CDMX, México

We construct the exact lens equation proposed by Frittelli *et al.* for the electrically charged static black hole spacetime of the Einstein-Euler-Heisenberg (EEH) theory, which is a nonlinear electromagnetic generalization of the Reissner-Nordström (RN) solution. We study the trajectories of light by means of the effective Plebański pseudometric. We compare the EEH exact lens equation with the thin-lens equations, as well as with the corresponding equations for the RN solution. The shadow of the black hole, the angular-diameter distance to the sources, and the time delay of arrival of the images are also calculated and discussed.

I. INTRODUCTION

In 1912 Mie put forward the first model for nonlinear electrodynamics [1]. Between 1932 and 1935 Born and Infeld proposed their nonlinear theory [2], where the field of a point charge turns out to be finite at $r = 0$, in contrast to the well-known $1/r^2$ singularity of the Coulomb field in Maxwell-Lorentz electrodynamics. Charged black hole solutions to the Einstein-Born-Infeld theory have been studied since the 1930s by Hoffmann [3], and later by Salazar *et al.* [4].

Then, Plebański postulated a class of nonlinear electro-dynamics [5], which contains the Born-Infeld theory as special case, where parity violating terms could arisen [6]. The characteristic surface depends on the field strength and the superposition principle for the electromagnetic field does not hold any longer. The coupling of the Einstein theory to the class of nonlinear electrodynamics proposed by Plebański admits regular black hole solutions, like the one obtained by Ayón-Beato *et al.* [7].

Moreover, quantum electrodynamical (QED) vacuum corrections to the Maxwell-Lorentz theory can be accounted for by an effective nonlinear theory derived by Euler and Heisenberg [8,9]. The vacuum is treated as a specific type of medium, the polarizability and magnet-izability properties of which are determined by the clouds of virtual charges surrounding the real currents and charges [10]. The weak field Euler-Heisenberg theory is the effective one of QED nonperturbative quantization after one loop. This theory is a valid physical theory [11], and a possible direct measurement of the Euler-Heisenberg effect has been proposed by Bordin *et al.* [12].

Recently, Ruffini *et al.* [13] considered the contributions of the Euler-Heisenberg effective Lagrangian in order to formulate the Einstein-Euler-Heisenberg theory and study the spherically symmetric black hole solutions endowed with electric and magnetic monopole charges. They reduced the problem to screened Reissner-Nordström solutions. A similar approach was studied by Yajima *et al.* 14]], in which the effective Euler-Heisenberg Langrangian is considered as the low-energy limit of the Born-Infeld theory and the nonlinearity parameters are treated as free parameters. They analyze either numerically or analytically the properties of spherically symmetric black holes sol-utions of the EEH theory. Additionally, Amaro *et al.* [15] considered an electrically charged static black hole solution to the EEH theory in terms of the Plebański dual variables, and studied all possible equatorial trajectories of test particles, as well as the shadow of the black hole for distant observers.

On the other hand, there exists currently a revival of interest in the concepts of *gravitational lensing* in strong fields and *black hole shadows*, since they are crucial for the interpretation of the relativistic images recently reported by the Event Horizon Telescope team from the supermassive black hole encountered at the nucleus of the galaxy M87 [16]. The *shadow* is bounded by the light ring, which contains at its center the *event horizon*. Then, it is possible to investigate the nearby regions outside it.

[*]amaro@xanum.uam.mx
[†]amac@xanum.uam.mx

There exist different gravitational lensing approaches [17], those built on the view that the lens is a perturbation of a background are known as thin-lens approaches, and they consider that the bending takes place only at the lens plane and that the light rays are otherwise straight lines. They also consider that the source and the observer are really far from the lens. The weak field thin-lens deals with small deflection angles. It corresponds to the standard study of gravitational lensing [18–20]. The strong field thin-lens was developed by Virbhadra et al. [21,22]. They assume that the bending angle is not necessarily small, so light rays may wind several times around the black hole.

The most general approach was developed by Frittelli et al. [23–26], and it is based on the exact study of the null geodesics followed by the light rays. In exact lens, the bending does not occur only in the lens plane, the locations of the observer and the source are not restricted. In [24], Frittelli et al. have shown that the exact lens equation in the case of strong fields is the most accurate gravitational lensing approach, since it respects the intrinsic nature of general relativity, i.e., covariance and nonlinearity.

The gravitational lensing for black hole solutions within nonlinear electrodynamics has been studied recently in [27–31]. In this paper, we construct the exact lens equation for the static, spherically symmetric, electrically charged EEH black hole spacetime, by following the approach of Frittelli et al. [23–26]. We also study the shadow of the black hole, the angular diameter distance, and the time delay of the signal.

The outline of the paper is as follows: The EEH theory is reviewed in Sec. II. The construction of an exact lens equation is revisited in Sec. III, in Sec. IV the exact lens equation for the EEH static black hole solution is presented and solved. Then, in Sec. V the exact and thin-lens results are compared. In Sec. VI the calculation of lensing observables is performed, while in Sec. VII the time delay of the images is studied. The summary and conclusions of the work are presented in Sec. VIII.

II. THE EINSTEIN-EULER-HEISENBERG THEORY

We revisit in this section the basic features of the Einstein theory coupled with the weak field approximation of the nonlinear electrodynamics proposed by Euler and Heisenberg [8], in the formalism introduced by Plebański [5].

The action for Einstein gravity minimally coupled to the Euler-Heisenberg theory reads [8,32]

$$
S = \frac{1}{16\pi G} \int_{M_4} d^4x \sqrt{-g} R
$$
$$
+ \frac{1}{4\pi} \int_{M_4} d^4x \sqrt{-g} \left(-X + \frac{2\alpha^2}{45m^4} \{4X^2 + 7Y^2\} \right), \quad (1)
$$

where R is the Ricci curvature scalar, G is the Newton's constant which we will take $G = 1$, m the electron mass,

and α the fine structure constant. The variables X and Y are the only two independent relativistic invariants constructed from the Maxwell field in four dimensions, which are defined as

$$
X = \frac{1}{4} F_{\mu\nu} F^{\mu\nu}, \qquad Y = \frac{1}{4} F_{\mu\nu}{}^*F^{\mu\nu}, \qquad (2)
$$

$^*F^{\mu\nu}$ is the dual of the Faraday tensor $F_{\mu\nu} = A_{\mu;\nu} - A_{\nu;\mu}$, and it is defined as usual $^*F^{\mu\nu} = \frac{1}{2\sqrt{-g}} \epsilon^{\mu\nu\sigma\rho} F_{\sigma\rho}$, and $\epsilon_{\mu\nu\sigma\rho}$ is the completely antisymmetric tensor that satisfies $\epsilon_{\mu\nu\sigma\rho} \epsilon^{\mu\nu\sigma\rho} = -4!$.

The equations of motion derived from this action are more easily written in terms of the Legendre dual description of nonlinear electrodynamics [5], which involves the introduction of the Plebański tensor $P_{\mu\nu}$ defined by

$$
dL(X, Y) = -\frac{1}{2} P^{\mu\nu} dF_{\mu\nu}, \qquad (3)
$$

where $L(X, Y)$ is the Lagrangian density for the Euler-Heisenberg nonlinear electrodynamics. In general it is defined as

$$
P_{\mu\nu} = -(L_X F_{\mu\nu} + L_Y{}^*F_{\mu\nu}), \qquad (4)
$$

where subscripts on L denote differentiation. Note that $P_{\mu\nu}$ coincides with $F_{\mu\nu}$ for the linear Maxwell theory. In our case it reads

$$
P_{\mu\nu} = F_{\mu\nu} - \frac{4\alpha^2}{45m^4} \{4X F_{\mu\nu} + 7Y^*F_{\mu\nu}\}. \qquad (5)
$$

The components of $P_{\mu\nu}$ are just the electric induction **D** and the magnetic field **H**, therefore Eq. (5) are the constitutive relations of the Euler-Heisenberg nonlinear electrodynamics. We denote by s and t the two independent invariants in terms of the dual Plebański variables $P_{\mu\nu}$, and are defined in the following way

$$
s = -\frac{1}{4} P_{\mu\nu} P^{\mu\nu}, \qquad t = -\frac{1}{4} P_{\mu\nu}{}^*P^{\mu\nu}, \qquad (6)
$$

where $^*P^{\mu\nu} = \frac{1}{2\sqrt{-g}} \epsilon^{\mu\nu\sigma\rho} P_{\sigma\rho}$.

The structural function $H(s, t)$ is written as

$$
H(s, t) = -\frac{1}{2} P^{\mu\nu} F_{\mu\nu} - L. \qquad (7)
$$

For the Euler-Heisenberg theory the structural function (to first order in α) reads

$$
H(s, t) = s - \frac{2\alpha^2}{45m^4} \{4s^2 + 7t^2\}. \qquad (8)
$$

The equations of motion for the coupled system are [4]

$$dF = 0, \qquad d^*P = 0, \qquad R_{\mu\nu} - \frac{1}{2}Rg_{\mu\nu} = 8\pi T_{\mu\nu}, \qquad (9)$$

with the energy-momentum tensor

$$T_{\mu\nu} = \frac{1}{4\pi}[H_s P_\mu{}^\beta P_{\nu\beta} + g_{\mu\nu}(2sH_s + tH_t - H)]. \qquad (10)$$

The energy-momentum tensor for the Euler-Heisenberg nonlinear electromagnetic field is given by

$$T_{\mu\nu} = \frac{1}{4\pi}\left[\left(1 - \frac{16\alpha^2}{45m^4}s\right)P_\mu{}^\beta P_{\nu\beta}\right.$$
$$\left. + g_{\mu\nu}\left(s - \frac{2\alpha^2}{45m^4}\{12s^2 + 7t^2\}\right)\right]. \qquad (11)$$

Setting $\alpha = 0$, it reduces to the standard linear Maxwell energy-momentum tensor.

III. THE EXACT LENS EQUATION

In this section we summarize the approach of Frittelli *et al.* [24], for the construction of a set of gravitational lens equations. A more general procedure can be found in [23,25].

Lets consider an observer whose coordinates are denoted by $x_0^a(\tau)$, where τ is the proper time. The observer measures light rays reaching him from past null geodesics, whose coordinates in the observer's celestial sphere are denoted by (η_1, η_2). The coordinates of the null geodesics x^a are parametrized by the affine parameter s, and satisfy the null geodesic equations. These local coordinates are functions of the observer's position, the celestial coordinates and the affine parameter, i.e., $x^a = x^a(x_0^a(\tau), \eta_1, \eta_2, s)$.

As usual, x^0 is a timelike coordinate, while x^i ($i = 1, 2, 3$) are spacelike. It is possible to perform the inversion $x^1(x_0^a(\tau), \eta_1, \eta_2, s) \to s(x_0^a(\tau), \eta_1, \eta_2, x^1)$, and we can reparametrize the geodesics in terms of x^1, for instance, as

$$x^0 = x^0(\tau, \eta_1, \eta_2, x^1), \qquad (12)$$

$$x^1 = x^1, \qquad (13)$$

$$x^A = x^A(\tau, \eta_1, \eta_2, x^1), \qquad A = 2, 3. \qquad (14)$$

When studying the trajectory of light, it is often used the backwards ray-tracing method, where the light ray travels from the observer to the source. Hence, the initial point is the observer's position x_0^a, while x^a determines the position of the source. The light ray arrives the observer's position at time τ and (η_1, η_2) direction in the observer's celestial sphere. In Fig. 1 the exact lens diagram is shown. If the value of x^1 can also be determined by observation, Eq. (12) corresponds to the exact time of arrival equation, while Eq. (14) corresponds to the exact lens equation.
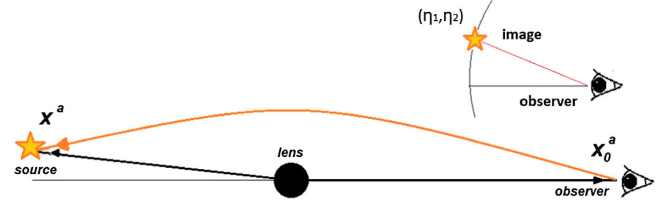
FIG. 1. The exact lens diagram. The light ray travels backwards in time, from the observer's position x_0^a to the source position x^a, with respect to the lens. The observer measures the image position with the celestial coordinates (η_1, η_2).

The spatial coordinate x^1 is often chosen as a radial coordinate, while the coordinates x^A are angular coordinates. Therefore, the exact lens equation, Eq. (14), gives us the angular position of the source. It corresponds to a map from the image angles (η_1, η_2) to the source angles (x^2, x^3), whose Jacobian reads

$$J(\tau, \eta_1, \eta_2, x^1) = \det \frac{\partial(x^2, x^3)}{\partial(\eta_1, \eta_2)}. \qquad (15)$$

$J = 0$ is a curve along which the mapping is not invertible. There might be an image in the direction $(\eta_1^{(1)}, \eta_2^{(1)})$ before reaching a caustic, and another image of the same source in the direction $(\hat{\eta}_1^{(2)}, \hat{\eta}_2^{(2)})$ beyond the caustic. $J = 0$ defines the caustics and separates regions where multiple images are seen.

The value of x^1 must be related to an observable, like the angular diameter distance. This is defined as $D_A(\tau, \eta_1, \eta_2, x^1) \equiv |dA_s/d\Omega_0|$, where dA_s is the infinitesimal area spanned by the observer's geodesic congruence at the position of the source [18], and the solid angle is $d\Omega_0 = K d\eta_1 d\eta_2$, with $K = K(\eta_1, \eta_2)$.

If we take the geodesic deviation vectors as

$$M_1^a = \frac{\partial x^a}{\partial \eta_1}, \qquad M_2^a = \frac{\partial x^a}{\partial \eta_2}, \qquad (16)$$

the area dA_s reads

$$dA_s = |2[(M_1 \cdot M_1)(M_2 \cdot M_2) - (M_1 \cdot M_2)^2]|^{1/2}d\eta_1 d\eta_2, \qquad (17)$$

where the dot means scalar product. The angular diameter distance is given by

$$D_A^2 = 2K^{-2}|(M_1 \cdot M_1)(M_2 \cdot M_2) - (M_1 \cdot M_2)^2|^{1/2}d\eta_1 d\eta_2. \qquad (18)$$

The value of D_A^2 is directly related to observable quantities, like the luminosity L, the apparent brightness of the source S, and the redshift z of the image, as follows

$$S = \frac{L}{4\pi(1+z)^4 D_A^2}. \qquad (19)$$

In the case in which multiple images are observed, D_A^2 is related to the relative magnification of the image

$$\mu_{12} = \frac{D_A^2(\eta_1^{(2)}, \eta_2^{(2)}, x^1)}{D_A^2(\hat{\eta}_1^{(1)}, \hat{\eta}_2^{(1)}, x^1)}, \qquad (20)$$

where the upper indices of (η_1, η_2) correspond to the observed image.

By observing the image of the source, η_1, η_2, and τ can be measured, while the angular diameter distance can be obtained from Eq. (19) or Eq. (20). Hence, with Eq. (18), the inversion $D_A(\tau, \eta_1, \eta_2, x^1) \to x^1(\tau, \eta_1, \eta_2, D_A)$ can be done, and Eq. (14) can be interpreted as the exact lens equation.

IV. THE EXACT LENS EQUATION FOR THE EINSTEIN-EULER-HEISENBERG BLACK HOLE

In this section, we construct the exact lens equation proposed by Frittelli *et al.* [23–26], for the static, spherically symmetric, electrically charged EEH black hole spacetime. In particular, we follow up the procedure presented in [24], i.e., we derive the black hole metric, compute the light equations of motion in terms of the image angles, study the conditions for the point of closest approach, introduce the angle Θ, and integrate the geodesic equations for the angular coordinates. The latter is detailed in Kling *et al.* [26].

A. Electrically charged static black hole solution

In order to present the Einstein-Euler-Heisenberg (EEH) generalization of the Reissner-Nordström solution, we consider the following static and spherically symmetric black hole metric [13,15]

$$ds^2 = -f(r)dt^2 + f(r)^{-1}dr^2 + r^2(d\theta^2 + \sin^2\theta d\phi^2), \quad (21)$$

with signature $\{-,+,+,+\}$ and $f(r) = 1-2m(r)/r$, and look for electrically charged black hole solutions. In [15], it is derived an electrically charged static black hole solution of the EEH theory in terms of the Plebański dual variables $P_{\mu\nu}$. We assume the following ansatz,

$$P_{\mu\nu} = \frac{Q}{r^2}(\delta_\mu^0 \delta_\nu^1 - \delta_\mu^1 \delta_\nu^0), \qquad (22)$$

which satisfies the electromagnetic equation (9). The electromagnetic invariants, Eq. (6), read

$$s = \frac{Q^2}{2r^4}, \qquad t = 0. \qquad (23)$$

The invariant s is $\frac{1}{2}\mathbf{D}^2$, and the pseudoinvariant t vanishes.

Integrating the Einstein equations, the mass-energy function $m(r)$ for the electrically charged static black hole solution is

$$m(r) = M - \frac{\tilde{Q}^2}{2r}, \qquad (24)$$

where the black hole charge is screened as

$$Q \to \tilde{Q} = Q\left(1 - \frac{\alpha}{225\pi}E_Q^2(r)\right)^{1/2}. \qquad (25)$$

When the electric field $E_Q(r) \equiv \frac{Q}{r^2 E_c}$ of the charged black hole is overcritical, electron-positron pair production takes place, and E_Q is screened down to its critical value $E_c \equiv \frac{m^2 c^3}{e\hbar}$. We use the units $\hbar = c = 1$ throughout this work. Notice that Eq. (24) behaves asymptotically ($r \to \infty$) as the Reissner-Nordström (RN) solution. Additionally, for $\alpha = 0$, we recover the linear RN solution. For $Q = 0$ it reduces to the Schwarzschild solution.

B. The light equations of motion

In linear Maxwell-Lorentz electrodynamics, the discontinuities of the field propagate according to the equation for the characteristic surfaces, $g^{\mu\nu}S_{,\mu}S_{,\nu} = 0$, which in standard optics is known as eikonal equation. The corresponding linear photons travel along null geodesics of the geometrical metric $g_{\mu\nu}$.

In Euler-Heisenberg nonlinear electrodynamics, photons propagate along null geodesics of the effective Plebański pseudometric $\gamma_{\mu\nu}$ [5] given by

$$\gamma^{\mu\nu} = g^{\mu\nu} + \frac{64\pi\alpha^2}{45m^4}T^{\mu\nu}, \qquad (26)$$

which differs from the geometrical metric $g_{\mu\nu}$, since it contains the energy-momentum tensor as well. The propagation equation for the nonlinear electromagnetic field discontinuities reads

$$\gamma^{\mu\nu}S_{,\mu}S_{,\nu} = 0, \qquad (27)$$

where $S_{,\mu}$ are the normal vectors to the characteristic surface S. Therefore, the energy-momentum tensor, $T_{\mu\nu}$ of the EH nonlinear field is responsible for the fact that these surfaces are not null surfaces of the geometrical metric. However, for $\alpha = 0$, i.e., linear Maxwell-Lorentz electrodynamics, both metrics coincide.

Hence, the null trajectories of nonlinear photons are obtained from the effective metric of Eq. (26). It is convenient to use the inverse radial coordinate

$$l = \frac{1}{\sqrt{2}r}. \tag{28}$$

Thus, the nonlinear photons satisfy the null condition

$$\gamma_{\mu\nu}\dot{x}^\mu \dot{x}^\nu = \left[g_{\mu\nu} - \frac{64\pi\alpha^2}{45m^4} T_{\mu\nu} \right] \dot{x}^\mu \dot{x}^\nu = 0, \tag{29}$$

and the following geodesic equations

$$\dot{t} = \left[1 - \frac{10\alpha}{225\pi} E_Q^2 \right] \frac{C}{\sqrt{2}f(l)}, \tag{30}$$

$$\dot{l} = \pm \left[1 - \frac{10\alpha}{225\pi} E_Q^2 \right] Cl^2 \sqrt{1 - \left[1 + \frac{20\alpha}{225\pi} E_Q^2 \right] \left(\frac{B}{C} \right)^2 l^2 f(l)}, \tag{31}$$

$$\left(\frac{\dot{\theta}}{l^2} \right)^2 = \left[1 + \frac{10\alpha}{225\pi} E_Q^2 \right]^2 \left(B^2 - \frac{A^2}{\sin^2\theta} \right), \tag{32}$$

$$\dot{\phi} = \left[1 + \frac{10\alpha}{225\pi} E_Q^2 \right] \frac{Al^2}{\sin^2\theta}. \tag{33}$$

The dot denotes derivative with respect to the affine parameter s. The constant of motion C is related to the energy of the photon and works as an scaling parameter of the effective potential. The constants A and B are related to the angular momentum of the photon and the Carter constant, respectively. They depend on the initial point, which in this case corresponds to the observer's location $(t_0, l_0, \theta_0, \phi_0)$.

It is important to notice that the electric field $E_Q \equiv 2Q^2 l^2 / E_c^2$ will be evaluated at a fixed l, depending on the particular case under consideration. For instance, in the case of the light ring, it is evaluated at the RN light ring, i.e., $E_Q(l_{c_{RN}}) = 2Q^2 l_{c_{RN}}^2 / E_c^2$. For the distance to the point of closest approach, $E_Q(l_{p_{RN}}) = 2Q^2 l_{p_{RN}}^2 / E_c^2$. At the observer's position, $E_Q(l_0) = 2Q^2 l_0^2 / E_c^2$.

The incident angle ψ that the null geodesic makes with the optical axis is defined by $\cot\psi = \sqrt{\gamma_{rr}}dr/(\sqrt{\gamma_{\theta\theta}}d\theta)$, while the azimuthal angle γ that the direction of the light ray makes around the optical axis is defined by $\cot\gamma = \sqrt{\gamma_{\theta\theta}}d\theta/(\sqrt{\gamma_{\phi\phi}}d\phi)$. At the observer's position, both are related to the constants of motion via

$$\left(\frac{B}{C} \right)^2 = \left[1 - \frac{20\alpha}{225\pi} E_Q^2(l_0) \right] \frac{\sin^2\psi}{l_0^2 f(l_0)}, \tag{34}$$

$$\left(\frac{A}{C} \right)^2 = \left[1 - \frac{20\alpha}{225\pi} E_Q^2(l_0) \right] \sin^2\theta_0 \sin^2\gamma \frac{\sin^2\psi}{l_0^2 f(l_0)}. \tag{35}$$

When the observer is far away from the black hole, $l_0 = 0$ and the nonlinear term $E_Q^2(l_0) = 0$. The nonlinear contribution becomes relevant for observers closer to the black

hole. The angles (γ, ψ) correspond to the image angles, while (θ, ϕ) correspond to the source angles. Equations (30)–(33) can be rewritten for $C = 1$, in terms of the observer's location and the image angles as

$$\dot{t} = \left[1 - \frac{10\alpha}{225\pi} E_Q^2 \right] \frac{1}{\sqrt{2}f(l)}, \tag{36}$$

$$\dot{l} = \pm \left[1 - \frac{10\alpha}{225\pi} E_Q^2 \right] l^2 \left\{ 1 - \left[1 + \frac{20\alpha}{225\pi} E_Q^2 \right] \left[1 - \frac{20\alpha}{225\pi} E_Q^2(l_0) \right] \right. $$
$$\left. \times \left(\frac{\sin^2\psi}{l_0^2 f(l_0)} \right) l^2 f(l) \right\}^{1/2}, \tag{37}$$

$$\left(\frac{\dot{\theta}}{l^2} \right)^2 = \left[1 + \frac{10\alpha}{225\pi} E_Q^2 \right]^2 \left[1 - \frac{20\alpha}{225\pi} E_Q^2(l_0) \right] $$
$$\times \left(\frac{\sin^2\psi}{l_0^2 f(l_0)} - \frac{(\sin\theta_0 \sin\gamma \sin\psi)^2}{l_0^2 f(l_0)\sin^2\theta} \right), \tag{38}$$

$$\dot{\phi} = \left[1 + \frac{10\alpha}{225\pi} E_Q^2 \right] \left[1 - \frac{10\alpha}{225\pi} E_Q^2(l_0) \right] $$
$$\times \frac{l^2 \sin\theta_0 \sin\gamma \sin\psi}{l_0 \sqrt{f(l_0)}\sin^2\theta}. \tag{39}$$

C. The point of closest approach, the light ring, and the shadow of the black hole

As mentioned above, the most efficient approach for studying light trajectories is the backwards ray-tracing method, where the light propagates from the observer backwards in time until reaching the source. First, the light ray points toward the black hole ($\dot{l} > 0$) until reaching the point to closest approach l_p. Then, it propagates outwards ($\dot{l} < 0$) in the direction of the source. The value of l_p is obtained from the condition $\dot{l} = 0$. Otherwise $\dot{l} \neq 0$, and the geodesics, Eqs. (36)–(39), can be reparametrized in terms of l.

If the light rays cross the unstable circular orbit (the light ring), they are trapped by the black hole. The position of the light ring is denoted by l_c and is obtained from the conditions $\dot{l} = 0$ and $\ddot{l} = 0$. These conditions can be computed from Eq. (37) and its derivative with respect to the affine parameter, while using $f(l) = 1 - 2\sqrt{2}Ml + 2\tilde{Q}^2 l^2$. Hence, l_c corresponds to the smaller root of the quadratic polynomial

$$1 - 3\sqrt{2}Ml_c + 4\tilde{Q}_c^2 l_c^2 = 0. \tag{40}$$

In order to compute the inverse radial distance of the EEH light ring (l_c), one should remember that the charge is screened at the inverse radial distance of the RN light ring ($l_{c_{RN}}$), namely

$$\tilde{Q}_c = Q\left(1 - \frac{\alpha}{225\pi} E_Q^2(l_{c_{RN}}) \right)^{1/2}, \tag{41}$$

where the electric field $E_Q(l_{c_{RN}}) \equiv 2Q^2 l_{c_{RN}}^2/E_c^2$. Thus,

$$l_c = \frac{3\sqrt{2}M}{8\tilde{Q}_c^2}\left(1 - \sqrt{1 - \frac{8}{9}\frac{\tilde{Q}_c^2}{M^2}}\right), \qquad (42)$$

with $l_{c_{RN}}$ being the radial distance of the linear case, i.e., Eq. (42) for $\alpha = 0$. The radius of the light ring is $r_c = 1/\sqrt{2}l_c$.

We are interested in light rays that do not cross the light ring, $l_p < l_c$. For these, the closest distant, which satisfies the condition $\dot{l} = 0$ on Eq. (37), is the smallest of the positive roots of

$$2\tilde{Q}_p^2 l_p^4 - 2\sqrt{2}M l_p^3 + l_p^2$$

$$-\frac{l_0^2(1 - 2\sqrt{2}M l_0 + 2\tilde{Q}_0^2 l_0^2)}{[1 + \frac{20\alpha}{225\pi}E_Q^2(l_{p_{RN}})][1 - \frac{20\alpha}{225\pi}E_Q^2(l_0)]\sin^2\psi} = 0. \quad (43)$$

The screened charges, $\tilde{Q}_0$ at the observer's position and $\tilde{Q}_p$ at the closest distance, are given by

$$\tilde{Q}_0 = Q\left(1 - \frac{\alpha}{225\pi}E_Q^2(l_0)\right)^{1/2}, \qquad (44)$$

$$\tilde{Q}_p = Q\left(1 - \frac{\alpha}{225\pi}E_Q^2(l_{p_{RN}})\right)^{1/2}, \qquad (45)$$

where $l_{p_{RN}}$ corresponds to the linear RN case of Eq. (43), for $l_{p_{RN}} < l_{c_{RN}}$. From Eqs. (43) and (34), with $C = 1$, one obtains the following useful relation

$$B^2 = \frac{1}{[1 + \frac{20\alpha}{225\pi}E_Q^2(l_{p_{RN}})]l_p^2(1 - 2\sqrt{2}M l_p + 2\tilde{Q}_p^2 l_p^2)}. \quad (46)$$

The light ring distance l_c is the critical value of the closest approach l_p. The corresponding critical incident angle ψ_c can be obtained from Eq. (43) for $l_p = l_c$. In order that a light ray is not trapped by the black hole [33], the incident angle must fulfill the condition $\sin^2\psi > \sin^2\psi_c$, with

$$\sin^2\psi_c = \frac{[1 - \frac{20\alpha}{225\pi}E_Q^2(l_{c_{RN}})]}{[1 - \frac{20\alpha}{225\pi}E_Q^2(l_0)]}\frac{l_0^2 f(l_0)}{l_c^2 f(l_c)}, \qquad (47)$$

where $f(l_c) = 1 - 2\sqrt{2}M l_c + 2\tilde{Q}_c^2 l_c^2$ with the screened charge, Eq. (41), and $f(l_0) = 1 - 2\sqrt{2}M l_0 + 2\tilde{Q}_0^2 l_0^2$ with $\tilde{Q}_0$, Eq. (44).

The radius of the black hole shadow r_{sh} is related to the critical angle: $r_{sh} = r_0 \tan\psi_c \approx r_0 \sin\psi_c$, for a small critical angle. From Eq. (47), the radius of the shadow of the EEH black hole reads

$$r_{sh} = \sqrt{\frac{1 - \frac{20\alpha}{225\pi}E_Q^2(l_{c_{RN}})}{1 - \frac{20\alpha}{225\pi}E_Q^2(l_0)}}\frac{\sqrt{f(l_0)}}{\sqrt{2}l_c\sqrt{f(l_c)}}, \qquad (48)$$

$$\approx \frac{[1 - \frac{10\alpha}{225\pi}E_Q^2(l_{c_{RN}})]}{\sqrt{2}l_c\sqrt{f(l_c)}}, \qquad (49)$$

for distant observers $(l_0 = 0)$, where $E_Q(0) = 0$ and $f(0) = 1$. Equation (49) is equivalent to the radius r_{sh} obtained in [15], while Eq. (48) is a more general result for observers not necessarily at infinity.

In Fig. 2 we show the radius of the shadows for the EEH and RN black holes at the observer's location. The respective asymptotes correspond to the case for the distant observer. The shadows for an observer at infinity and an observer at the innermost stable circular orbit (ISCO) are shown in Fig. 3. The EEH shadow is always inside the RN one as in [15], where we display the shadow radius varying the values of Q and M.
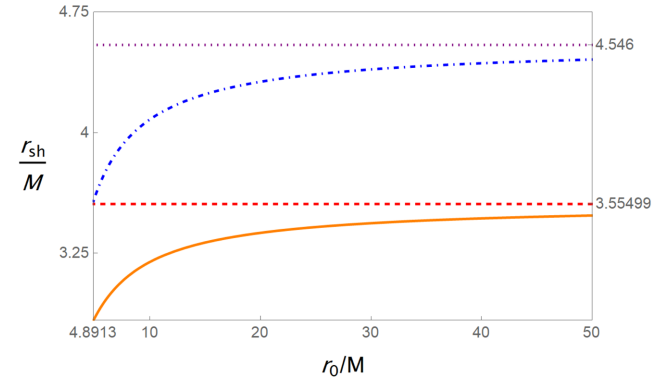
FIG. 2. The radius of the shadows for fixed $M = 10^4 M_\odot$ and $Q = 0.8M$. The continuous line corresponds to the EEH shadow as function of r_0. Its asymptote is the dashed line at $r_{sh} = 3.55499M$. The dot-dashed line corresponds to the RN shadow. Its asymptote is the dotted line at $r_{sh_{RN}} = 4.546M$.
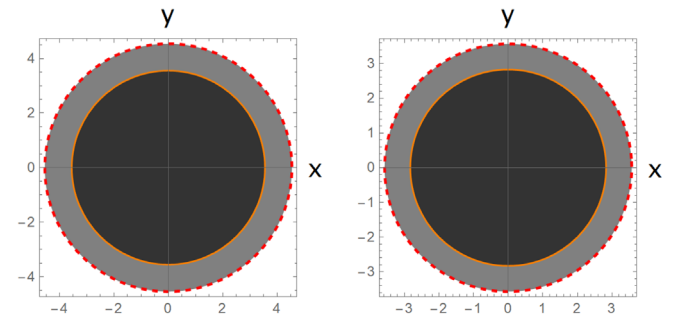
FIG. 3. The shadows for fixed $M = 10^4 M_\odot$ and $Q = 0.8M$. The left-hand side (lhs) corresponds to $r_0 \to \infty$, while the right-hand side (rhs) corresponds to $r_0 = 4.8913M$, at the ISCO. In both cases, the EEH shadow (darker circle) lies inside the RN one (fainter circle).

D. The integration of the angular coordinates

In order to integrate the geodesic equations for the angular coordinates (θ, ϕ), we introduce an angle Θ. From Eq. (34), Eq. (39), and Eq. (38), it is given by $\dot{\Theta}^2 \equiv \dot{\theta}^2 + \sin^2\theta\,\dot{\phi}^2 = [1 + \frac{10\alpha}{225\pi}E_Q^2]l^2 B$. First, we integrate the geodesic equations in the x–z plane [26], where $\phi = 0$ and Θ goes from 0 to 2π. The initial point is the observer's position on this plane, $\tilde{x}_0^a = (t_0, l_0, \theta_0 = \pi, \phi_0 = 0)$, while the end point is $x^a = (t, l, \Theta, \phi = 0)$. Hence, $\Theta_0 = \pi$. By means of Eq. (37) together with Eq. (43), the solution to the angular component of the geodesic equation on the x–z plane reads

$$\phi = 0, \quad \Theta = \pi - \int_{l_0}^{l} \frac{\pm[1 + \frac{20\alpha}{225\pi}E_Q^2]dl'}{\sqrt{\frac{1}{B^2} - [1 + \frac{20\alpha}{225\pi}E_Q^2]l'^2 f(l')}}, \quad (50)$$

with B given by Eq. (46) and $f(l') = 1 - 2\sqrt{2}Ml' + 2l'^2\tilde{Q}^2$. The sign depends on the radial direction of the light ray.

The trajectory of the light ray within the backwards ray-tracing method, can be divided in two patches. First, the ray comes inwards from l_0 to l_p. Then, it goes backwards from l_p to the source at l_s. Thus, $\Theta(l_s, l_0, l_p)$ reads

$$\Theta = \pm\left(\pi - \int_{l_0}^{l_p} \frac{2[1 + \frac{20\alpha}{225\pi}E_{Q_+}^2]dl'}{\sqrt{\frac{1}{B^2} - [1 + \frac{20\alpha}{225\pi}E_{Q_+}^2]l'^2(1 - 2\sqrt{2}Ml' + 2l'^2\tilde{Q}^2)}} \right.$$
$$\left. - \int_{l_s}^{l_0} \frac{[1 + \frac{20\alpha}{225\pi}E_{Q_-}^2]dl'}{\sqrt{\frac{1}{B^2} - [1 + \frac{20\alpha}{225\pi}E_{Q_-}^2]l'^2(1 - 2\sqrt{2}Ml' + 2l'^2\tilde{Q}^2)}} \right). \quad (51)$$

Since the effective weak field Euler-Heisenberg nonlinear electrodynamics of QED is valid only for constant fields [13], Eq. (51) should be integrated considering E_Q as a constant. For numerical integrations, it can be evaluated on the middle point, $E_{Q_+} = E_{Q_+}([l_0 + l_p]/2)$ in the first integral, and $E_{Q_-} = E_{Q_-}([l_s + l_0]/2)$ in the second one.

Equation (51) depends on the incident angle ψ through the point of closest approach l_p. A plot of Θ for fixed l_0 and l_s is shown in Fig. 4. The asymptote corresponds to the critical angle ψ_c. The closer the rays approach to the light ring, more turns around the black hole they make.

The integration on the x–z plane, Eq. (50), is generalized through a rotation from an arbitrary initial point $x_0^a = (t_0, l_0, \theta_0, \phi_0)$. The angle Θ is constant along the rotation. It is convenient to introduce the complex stereographic variable $\zeta = \cot\frac{\theta}{2}e^{i\phi}$ and its complex conjugate $\bar{\zeta} = \cot\frac{\theta}{2}e^{-i\phi}$. Therefore, the rotation corresponds to the $SU(2)$ transformation $\zeta' = \frac{a\cot\frac{\Theta}{2} + b}{c\cot\frac{\Theta}{2} + d}$, where a, b, c, and d are the Cayley-Klein parameters. They can be written in terms of the Euler
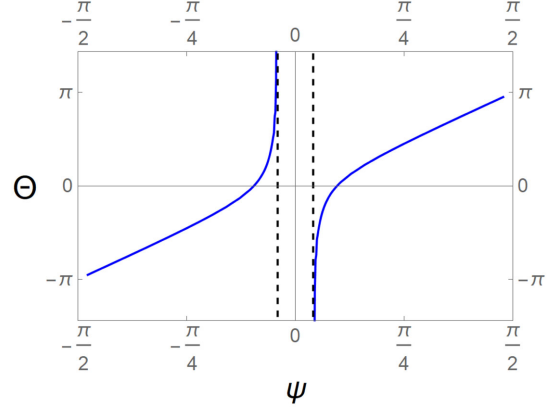
FIG. 4. The continuous line corresponds to Θ, Eq. (51), while the dashed line corresponds to ψ_c, Eq. (47). The parameters are: $M = 10^4\,M_\odot$, $Q = 0.8M$, and $r_0 = r_s = 30M$.

angles [34], with respect to the initial point. In terms of the initial point angular coordinates,

$$\zeta = e^{i\phi_0}\left(\frac{\cot\frac{\theta_0}{2} + e^{i\gamma}\cot\frac{\Theta(l, l_0, l_p)}{2}}{1 - e^{i\gamma}\cot\frac{\theta_0}{2}\cot\frac{\Theta(l, l_0, l_p)}{2}}\right). \quad (52)$$

Hence, in terms of the standard spherical coordinates (θ, ϕ),

$$\cos\theta = -\cos\theta_0\cos\Theta + \sin\theta_0\sin\Theta\cos\gamma,$$
$$\tan\phi = \frac{\sin\phi_0\sin\theta_0 - \tan\Theta(\cos\phi_0\sin\gamma - \sin\phi_0\cos\gamma\cos\theta_0)}{\cos\phi_0\sin\theta_0 + \tan\Theta(\sin\phi_0\sin\gamma + \cos\phi_0\cos\gamma\cos\theta_0)}. \quad (53)$$

If the observer's location (l_0, θ_0, ϕ_0), the angular position of the image (γ, ψ), and the angle $\Theta(l_s, l_0, \psi)$, Eq. (51), are known, we are able to compute the real angular position of the source, (θ, ϕ). Thus, Eq. (53) can be interpreted as the exact lens equation for the EEH black hole, since the inversion $l_s(x_0^a, \gamma, \psi, s) \rightarrow s(x_0^a, \gamma, \psi, l_s)$ can be done by integrating Eq. (31) and using Eq. (46), i.e.,

$$s = 2\int_{l_0}^{l_p}\sqrt{\frac{l_p^2 f(l_p)}{l_p^2 f(l_p) - \left[\frac{1 + \frac{20\alpha}{225\pi}E_{Q_+}^2}{1 + \frac{20\alpha}{225\pi}E_Q^2(l_{pRN})}\right]l^2 f(l)}}\left[1 + \frac{10\alpha}{225\pi}E_{Q_+}^2\right]\frac{dl}{l^2}$$
$$+ \int_{l_s}^{l_0}\sqrt{\frac{l_p^2 f(l_p)}{l_p^2 f(l_p) - \left[\frac{1 + \frac{20\alpha}{225\pi}E_{Q_-}^2}{1 + \frac{20\alpha}{225\pi}E_Q^2(l_{pRN})}\right]l^2 f(l)}}\left[1 + \frac{10\alpha}{225\pi}E_{Q_-}^2\right]\frac{dl}{l^2}. \quad (54)$$

For the particular case in which the observer is located along the z-axis, $\theta_0 = \pi$ and $\phi_0 = 0$, Eq. (53) reduces to $\cos\theta = \cos\Theta$, and the exact lens equation is

$$\theta = \Theta(l_s, l_0, l_p). \quad (55)$$
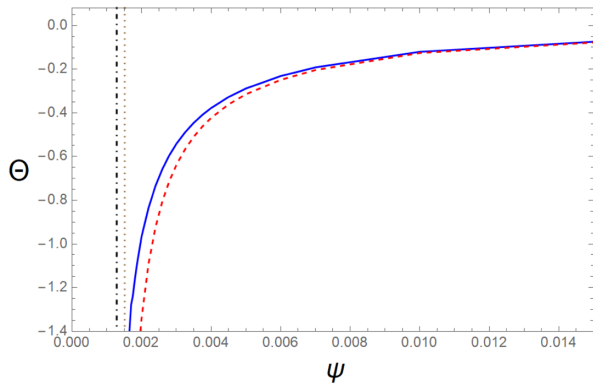
FIG. 5. The angle Θ, Eq. (51), as a function of the incident angle ψ for the EEH black hole (continuous line) and that for the RN linear case (dashed line) are displayed. The dot-dashed line corresponds to the critical incident angle ψ_c, Eq. (47), while the dotted line corresponds to that of the linear case $\alpha = 0$. The parameters are: $M = 10^4 \, M_\odot$, $Q = 0.8M$, and $r_0 = r_s = 3000M$.

In Fig. 5 the angle Θ for the EEH black hole and for the RN one is shown. For large image angles ψ the difference is barely visible, but the difference becomes relevant for values of the image angle closer to ψ_c. For the case $\theta = \Theta$, this difference would correspond to a different source angular location.

V. COMPARISON WITH THE THIN-LENS EQUATIONS

The exact lens equation, Eq. (53), has been computed following [24], by means of the study of the trajectory of the light ray along the null geodesic. However, as mentioned above, there exist other approaches for studying gravitational lensing, like the thin-lens approaches, in which the bending takes place at the lens plane. The source and the observer are on the same plane.

In Fig. 6, the thin-lens diagram is shown. D_s is the distance from the observer to the source plane, while D_d is that to the lens plane. The angular position of the source is β, and that for the image is ψ. The latter is the apparent location of the source and corresponds to the incident angle of the light ray at the observer's position.

D_{ds} is the distance of the source plane measured from the lens plane. The angular position of the source with respect to the black hole is θ, and the bending angle is $\hat{\sigma}$. In the framework of the thin-lens approach, the deflection angle of the weak-field thin-lens is small, while in the strong-field thin-lens the bending angle increases to infinity as the rays approach the unstable circular orbit [21,22].

A. Strong-field thin-lens equation

From the geometry of the lens diagram, Fig. 6, the strong-field thin-lens equation reads [21]
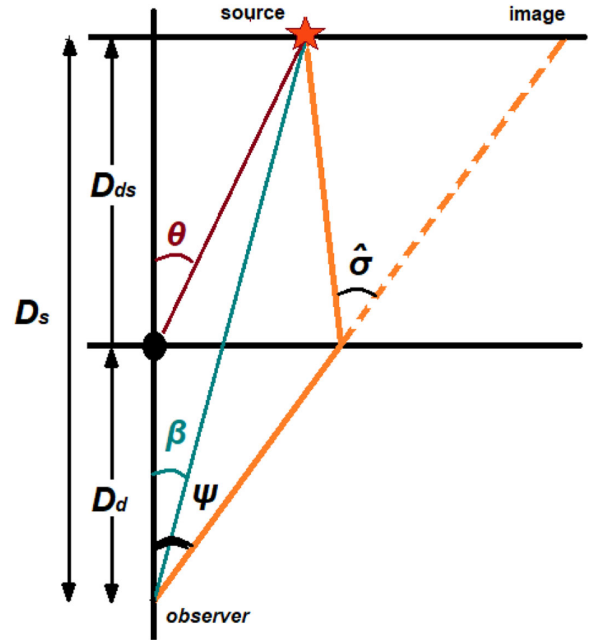
FIG. 6. The thin-lens diagram.

$$\tan \beta = \tan \psi - \frac{D_{ds}}{D_s} [\tan \psi + \tan (\hat{\sigma} - \psi)]. \quad (56)$$

Since in the thin-lens approach both the source and the observer lie at infinity, the total change on θ of a light ray which travels from the source to the observer is twice the change from ∞ to the closest distance r_p [35]. Notice that without deflection, the total angular change would be π, which corresponds to a straight line. Therefore, the deflection angle $\hat{\sigma}$ in terms of the inverse radial coordinate l is given by

$$\hat{\sigma} = 2 \int_0^{l_p} \frac{[1 + \frac{20\alpha}{225\pi} E_Q^2(l_p/2)] dl'}{\sqrt{\frac{1}{B^2} - [1 + \frac{20\alpha}{225\pi} E_Q^2(l_p/2)] l'^2 f(l')}} - \pi, \quad (57)$$

with the constant B, Eq. (46), and $f(l') = 1 - 2\sqrt{2}Ml' + 2\tilde{Q}^2 l'^2$.

In order to compare Eq. (56) with the corresponding exact lens equation, Eq. (55), we must analyze each of the terms. From Eq. (57) and Eq. (51), it is straightforward to see that

$$\hat{\sigma} = -\Theta(l_s, l_0, \psi)|_{l_s = l_0 = 0}. \quad (58)$$

Introducing the inverse radial coordinate, from Fig. 6 it is easy to check that

$$\tan \beta = \frac{D_{ds}}{D_s} \tan \theta, \quad (59)$$

$$D_d = \frac{1}{\sqrt{2} l_0}, \quad (60)$$

$$D_{ds} = \frac{\cos\theta}{\sqrt{2}l_s}, \tag{61}$$

$$D_s = \frac{1}{\sqrt{2}l_0} + \frac{\cos\theta}{\sqrt{2}l_s}. \tag{62}$$

Replacing Eqs. (58)–(62) into Eq. (56), one obtains the strong-field thin-lens equation:

$$\theta = \psi + \Theta|_{l_s=l_0=0} + \arcsin\left[\frac{l_s}{l_0}\tan\psi\cos\left(\Theta|_{l_s=l_0=0} + \psi\right)\right]. \tag{63}$$

B. Weak-field thin-lens equation

In the weak-field thin-lens approximation, the angles β, ψ, and α, are assumed to be small, i.e., $\tan x \approx x$. Hence, Eq. (56) for the weak-field thin-lens becomes

$$\beta = \psi - \frac{D_{ds}}{D_s}\hat{\sigma}. \tag{64}$$

In this case, the deflection angle can be obtained from the Robertson expansion and integration of Eq. (57), where it is assumed that the distance to the point of closest approach is much bigger than the mass of the black hole [35], i.e., $r_p \gg 2M$. Additionally, since the EEH solution behaves asymptotically as the RN one, the corresponding points of closest approach are practically equal, $r_{p_{RN}} \approx r_p$. Furthermore, the weak-field deflection angle, up to first order in α and to second order in M/r_p, reads

$$\hat{\sigma} = \frac{4M}{r_p} + \frac{4M^2}{r_p^2}\left(\frac{15\pi}{16} - 1\right) - \frac{3\pi Q^2}{4r_p^2}$$
$$+ \frac{10\alpha}{225\pi}E_Q^2(r_p)\left[\frac{4M}{r_p} + \frac{10M^2}{r_p^2}\left(\frac{3\pi}{4} - 1\right) - \frac{3\pi Q^2}{2r_p^2}\right]. \tag{65}$$

The thin-lens deflection angle for the RN solution has been studied in [36,37], while for the EEH solution in [29,30]. Moreover, Eq. (65) has been computed in the framework of the QED interpretation of the weak field Euler-Heisenberg theory, by means of the effective Plebański pseudometric $\gamma^{\mu\nu}$.

In order to write Eq. (65) in terms of a small incident angle ψ, $r_p = D_d\tan\psi \approx D_d\psi$, Fig. 6, Eqs. (59)–(62) read

$$\beta = \frac{D_{ds}}{D_s}\theta, \tag{66}$$

$$D_d = \frac{1}{\sqrt{2}l_0}, \tag{67}$$

$$D_{ds} = \frac{1}{\sqrt{2}l_s}, \tag{68}$$

$$D_s = \frac{1}{\sqrt{2}l_0} + \frac{1}{\sqrt{2}l_s}. \tag{69}$$
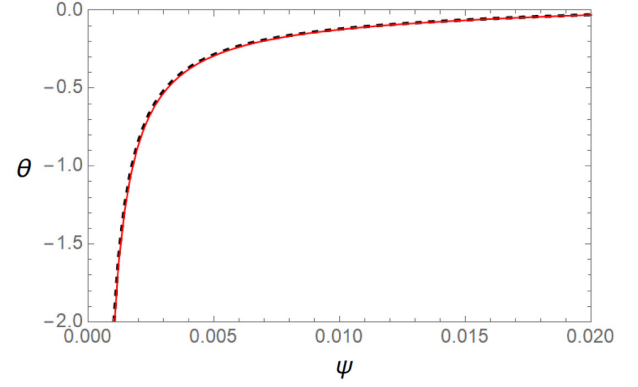
FIG. 7. The source angle θ, Eq. (70), as a function of the incident angle ψ for the EEH black hole (continuous line), and the RN case (dashed line), are presented. The parameters are $M = 10^4\ M_\odot$, $Q = 0.8M$, and $r_0 = r_s = 3000M$.

Replacing $r_p = \psi/\sqrt{2}l_0$, the weak-field thin-lens equation is given by

$$\theta = \frac{l_s + l_0}{l_0}\left(\psi - \frac{4\sqrt{2}M}{\psi}\frac{l_0^2}{l_s + l_0}\right.$$
$$- \left[\frac{8M^2}{\psi^2}\left(\frac{15\pi}{16} - 1\right) - \frac{3\pi Q^2}{2\psi^2}\right]\frac{l_0^3}{l_s + l_0}$$
$$- \frac{10\alpha}{225\pi}E_Q^2(r_p)\left\{\frac{4\sqrt{2}M}{\psi}\frac{l_0^2}{l_s + l_0}\right.$$
$$\left.\left. + \left[\frac{20M^2}{\psi^2}\left(\frac{3\pi}{4} - 1\right) - \frac{3\pi Q^2}{\psi^2}\right]\frac{l_0^3}{l_s + l_0}\right\}\right). \tag{70}$$

In Fig. 7, the weak-field source angle θ, Eq. (70), as a function of ψ is presented for the EEH and RN cases. The Euler-Heisenberg effect is not relevant, since both the observer and the source are located far away from the black hole ($r_0 = r_s = 3000M$). Nevertheless, for the exact source angle θ, Eq. (55), the nonlinear effect becomes relevant for small image angles ψ, as shown in Fig. 5. The weak field thin-lens and the exact source angles are plotted in Fig. 8.

VI. OBSERVABLES

Equation (53) can be interpreted as the exact lens equation if the value of the inverse radial parameter l is related to an observable. In order to obtain the exact expression of the angular diameter distance, Eq. (18), we must compute the connecting vectors, Eq. (16), which for the coordinates $x^a = (t, l, \theta, \phi)$ and image angles (γ, ψ), read

$$M_1^a = \left(0, 0, \frac{\partial\theta}{\partial\gamma}, \frac{\partial\phi}{\partial\gamma}\right), \tag{71}$$

$$M_2^a = \left(\frac{\partial t}{\partial\psi}, 0, \frac{\partial\theta}{\partial\psi}, \frac{\partial\phi}{\partial\psi}\right). \tag{72}$$
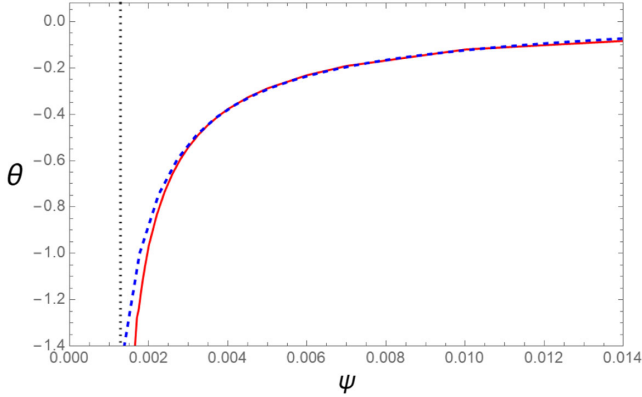
FIG. 8. We display the source angle θ, as a function of the incident angle ψ, from the exact lens equation (continuous line), Eq. (55), together with the one of the weak-field thin-lens equation (dashed line), Eq. (70). The dotted line corresponds to the asymptote ψ_c, Eq. (47). The parameters are $M = 10^4 \, M_\odot$, $Q = 0.8M$, and $r_0 = r_s = 3000M$.

Performing the following partial derivatives, Eq. (53), one obtains

$$\frac{\partial \theta}{\partial \gamma} = \frac{\sin \theta_0 \sin \Theta \sin \gamma}{\sin \theta}, \tag{73}$$

$$\frac{\partial \theta}{\partial \psi} = -\frac{\cos \theta_0 \sin \Theta + \sin \theta_0 \cos \Theta \cos \gamma}{\sin \theta} \frac{\partial \Theta}{\partial \psi}, \tag{74}$$

$$\frac{\partial \phi}{\partial \gamma} = -\frac{\sin \Theta (\sin \Theta \cos \theta_0 + \cos \Theta \sin \theta_0 \cos \gamma)}{\sin^2 \theta}, \tag{75}$$

$$\frac{\partial \phi}{\partial \psi} = -\frac{\sin \theta_0 \sin \gamma}{\sin^2 \theta} \frac{\partial \Theta}{\partial \psi}. \tag{76}$$

Since in Euler-Heisenberg nonlinear electrodynamics light propagates along null geodesics of the effective Plebański pseudometric, Eq. (26), the products of the connecting vectors are given by

$$M_1 \cdot M_1 = \frac{[1 - \frac{10\alpha}{225\pi} E_Q^2]}{2l^2} \left[\left(\frac{\partial \theta}{\partial \gamma} \right)^2 + \sin^2 \theta \left(\frac{\partial \phi}{\partial \gamma} \right)^2 \right], \tag{77}$$

$$M_2 \cdot M_2 = -\left[1 + \frac{10\alpha}{225\pi} E_Q^2 \right] f(l) \left(\frac{\partial t}{\partial \psi} \right)^2$$
$$+ \frac{[1 - \frac{10\alpha}{225\pi} E_Q^2]}{2l^2} \left[\left(\frac{\partial \theta}{\partial \psi} \right)^2 + \sin^2 \theta \left(\frac{\partial \phi}{\partial \psi} \right)^2 \right], \tag{78}$$

$$M_1 \cdot M_2 = \frac{[1 - \frac{10\alpha}{225\pi} E_Q^2]}{2l^2} \left[\left(\frac{\partial \theta}{\partial \gamma} \right) \left(\frac{\partial \theta}{\partial \psi} \right) + \sin^2 \theta \left(\frac{\partial \phi}{\partial \gamma} \right) \left(\frac{\partial \phi}{\partial \psi} \right) \right]. \tag{79}$$

Hence, from Eq. (17), the area dA_s becomes

$$dA_s = \left(\left[1 - \frac{10\alpha}{225\pi} E_Q^2 \right]^2 \frac{\sin^2 \theta}{4l^4} \left[\frac{\partial \theta}{\partial \gamma} \frac{\partial \phi}{\partial \psi} - \frac{\partial \phi}{\partial \gamma} \frac{\partial \theta}{\partial \psi} \right]^2 \right.$$
$$\left. - \left[1 + \frac{10\alpha}{225\pi} E_Q^2 \right] f(l) \left(\frac{\partial t}{\partial \psi} \right)^2 M_1 \cdot M_1 \right)^{1/2} d\gamma d\psi. \tag{80}$$

The first term is identified as the Jacobian of the map from the image angles (γ, ψ) to the source angles (θ, ϕ), as defined in Eq. (15). By means of Eqs. (73)–(76), it can be written as $J = -(\sin \Theta / \sin \theta) \partial \Theta / \partial \psi$, and the product of the second term reduces to $M_1 \cdot M_1 = [1 - \frac{10\alpha}{225\pi} E_Q^2] \sin^2 \Theta / 2l^2$. Therefore, the area dA_s reduces to

$$dA_s = \frac{\sin \Theta}{2l^2} \left(\left[1 - \frac{10\alpha}{225\pi} E_Q^2 \right]^2 \left(\frac{\partial \Theta}{\partial \psi} \right)^2 \right.$$
$$\left. - 2l^2 f(l) \left(\frac{\partial t}{\partial \psi} \right)^2 \right)^{1/2} d\gamma d\psi. \tag{81}$$

At the observer's location, the solid angle is given in terms of the image angles as $d\Omega_0 = \sin \psi \, d\psi \, d\gamma$. Thus, the angular diameter distance becomes

$$D_A^2 = \frac{\sin \Theta}{2l^2 \sin \psi} \left(\left[1 - \frac{10\alpha}{225\pi} E_Q^2 \right]^2 \left(\frac{\partial \Theta}{\partial \psi} \right)^2 - 2l^2 f(l) \left(\frac{\partial t}{\partial \psi} \right)^2 \right)^{1/2}. \tag{82}$$

The derivative $\partial t / \partial \psi$ results to be proportional to $\partial \Theta / \partial \psi$. The components of the null vector tangent to the light rays are $l^a \equiv (\dot{t}, \dot{l}, \dot{\theta}, \dot{\phi})$, and the orthogonality condition is $\gamma_{ab} M_2^a l^b = 0$. Both connecting vectors M_1^a and M_2^a are orthogonal to l^a. By using the geodesic equations for θ and ϕ, Eq. (38) and Eq. (39) respectively, as well as the explicit expressions Eq. (74) and Eq. (76), the following expression is obtained:

$$\frac{\partial t}{\partial \psi} = -\frac{[1 - \frac{10\alpha}{225\pi} E_Q^2(l_0)]}{[1 + \frac{10\alpha}{225\pi} E_Q^2]} \frac{\sin \psi}{\sqrt{2l_0^2 f(l_0)}} \frac{\partial \Theta}{\partial \psi}. \tag{83}$$

Replacing Eq. (83) into Eq. (81) and Eq. (82), the area and the angular-diameter distance reduce to

$$dA_s = \left[1 - \frac{10\alpha}{225\pi} E_Q^2 \right] \frac{\sin \Theta}{2l^2} \left| \frac{\partial \Theta}{\partial \psi} \right|$$
$$\times \left(1 - \left[1 - \frac{10\alpha}{225\pi} E_Q^2(l_0) \right]^2 \sin^2 \psi \frac{l^2 f(l)}{l_0^2 f(l_0)} \right)^{1/2} d\gamma d\psi, \tag{84}$$

$$D_A^2 = \left[1 - \frac{10\alpha}{225\pi} E_Q^2 \right] \frac{\sin \Theta}{2l^2 \sin \psi} \left| \frac{\partial \Theta}{\partial \psi} \right|$$
$$\times \left(1 - \left[1 - \frac{10\alpha}{225\pi} E_Q^2(l_0) \right]^2 \sin^2 \psi \frac{l^2 f(l)}{l_0^2 f(l_0)} \right)^{1/2}, \tag{85}$$

respectively. Eq. (85) provides the angular diameter distance in terms of the inverse radial parameter l. If $l = l_s$ is the source position, the inversion $D_A(x_0^a, \gamma, \psi, l_s) \to l_s(x_0^a, \gamma, \psi, D_A)$ can be done numerically.

By observation of the imaging, using Eq. (19) or Eq. (20), it is possible to determine D_A and the angles

(γ, ψ). By computing the right hand side of Eq. (85) for fixed l_0 and by using the known D_A from observation, one obtains the value of l_s. In order to do it, we employ the exact expression, Eq. (51), and $\partial \Theta / \partial l_p$. Using the Leibniz integral rule,

$$
\frac{\partial \Theta}{\partial l_p} = \lim_{\epsilon \to 0} \left\{ \int_{l_0}^{l_p - \epsilon} \frac{2[1 + \frac{20\alpha}{225\pi} E_{Q_+}^2][1 + \frac{20\alpha}{225\pi} E_Q^2(l_{p_{\mathrm{RN}}})] l_p (1 - 3\sqrt{2} M l_p + 4 l_p^2 \tilde{Q}_p^2) dl'}{([1 + \frac{20\alpha}{225\pi} E_Q^2(l_{p_{\mathrm{RN}}})] l_p^2 f(l_p) - [1 + \frac{20\alpha}{225\pi} E_{Q_+}^2] l'^2 f(l'))^{3/2}} \right.
$$
$$
\left. - \frac{2[1 + \frac{20\alpha}{225\pi} E_{Q_+}^2]}{\sqrt{[1 + \frac{20\alpha}{225\pi} E_Q^2(l_{p_{\mathrm{RN}}})] l_p^2 f(l_p) - [1 + \frac{20\alpha}{225\pi} E_{Q_+}^2] l'^2 f(l')}} \bigg|_{l' = l_p - \epsilon} \right\}
$$
$$
+ \int_{l_s}^{l_0} \frac{[1 + \frac{20\alpha}{225\pi} E_{Q_-}^2][1 + \frac{20\alpha}{225\pi} E_Q^2(l_{p_{\mathrm{RN}}})] l_p (1 - 3\sqrt{2} M l_p + 4 l_p^2 \tilde{Q}_p^2) dl'}{([1 + \frac{20\alpha}{225\pi} E_Q^2(l_{p_{\mathrm{RN}}})] l_p^2 f(l_p) - [1 + \frac{20\alpha}{225\pi} E_{Q_-}^2] l'^2 f(l'))^{3/2}}. \tag{86}
$$

VII. TIME DELAY

In this section, we integrate the geodesic equation for the t coordinate, which allows us to derive the exact equation of the arrival time. By means of Eq. (46), the geodesic equation, Eq. (30), integrates as follows,

$$
t = 2 \int_{l_0}^{l_p} \sqrt{\frac{l_p^2 f(l_p)}{l_p^2 f(l_p) - \left[\frac{1 + \frac{20\alpha}{225\pi} E_{Q_+}^2}{1 + \frac{20\alpha}{225\pi} E_Q^2(l_{p_{\mathrm{RN}}})}\right] l^2 f(l)}} \frac{dl}{\sqrt{2} l^2 f(l)}
$$
$$
+ \int_{l_s}^{l_0} \sqrt{\frac{l_p^2 f(l_p)}{l_p^2 f(l_p) - \left[\frac{1 + \frac{20\alpha}{225\pi} E_{Q_-}^2}{1 + \frac{20\alpha}{225\pi} E_Q^2(l_{p_{\mathrm{RN}}})}\right] l^2 f(l)}} \frac{dl}{\sqrt{2} l^2 f(l)}. \tag{87}
$$

Equation (87) is the exact equation of arrival time.
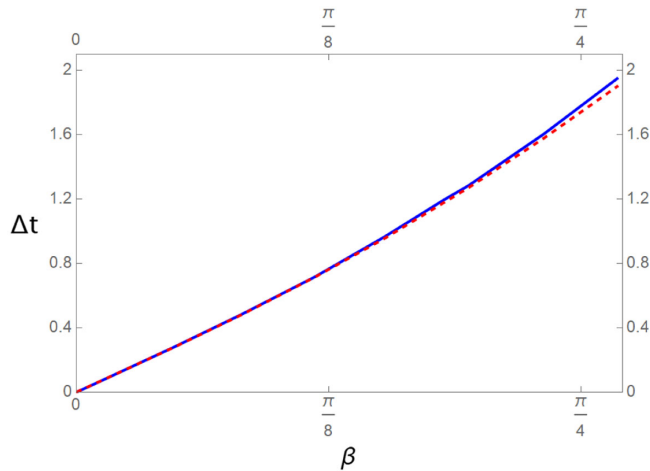
FIG. 9. The exact time delay in seconds as a function of the source angle β in radians, for the EEH black hole (continuous line), and that for the RN case (dashed line) are displayed. The parameters are $M = 10^4 \, M_\odot$, $Q = 0.8M$, $r_0 = r_s = 30M$.

We are interested in the case in which two light rays from the same source reach the observer, i.e., when two images with their respective image angle ψ are observed. The difference between the time of arrival of each light ray, Δt, corresponds to the exact time delay.

In Fig. 9 the exact time delay as a function of β is presented. As the distance of the source from the optical axis increases, bigger is the time delay. When the source, the lens, and the observer lie along the same line, $\Delta t = 0$, as expected from symmetry. The EEH effect on the time delay is barely visible when compared with the RN case, since these light rays do not wind around the black hole. For more distant observers, the difference is even smaller.

VIII. SUMMARY AND CONCLUSIONS

We consider the effective QED theory after one-loop, i.e., the weak field Euler-Heisenberg nonlinear electrodynamics [8], where the vacuum is treated as a specific type of medium, the polarizability properties of which are determined by the clouds of virtual charges surrounding the real ones. The Einstein-Euler-Heisenberg generalization of the Reissner-Nordström black hole solution includes the screening effect of the black hole charge [13,15]. We study the light trajectories by means of the effective Plebański pseudometric, which contains the energy-momentum tensor of the nonlinear Euler-Heisenberg electromagnetic field [5]. We derive the exact lens equation for the EEH solution, following Frittelli et al. [23–25].

The geodesic equations are written in terms of the incident angle of the light ray at the observer's position, as well as in terms of the azimuthal angle that the direction of the light ray makes around the optical axis. We analyze the distance to the point of closest approach, with the light ring distance being its critical value. We integrate the geodesic equations for the angular coordinates on the x–z plane. This

integration is generalized through a rotation to an arbitrary initial point by using the complex stereographic variables.

We obtain the EEH exact lens equation and compare it with the corresponding thin-lens equations. The differences with the linear RN case are discussed. The effect of the Euler-Heisenberg nonlinear electrodynamics becomes relevant for light rays which approach closer to the light ring, when the bending angle increases to infinity. Although the difference is barely visible, due to the large distances involved, it would correspond to a different real location of the source. The effects increase for observers closer to the lens, however, they are not realistic observers.

We also study the shadow of the EEH black hole, which lays always inside the RN one. We compute the angular-diameter distance related to observable quantities, like the luminosity, the apparent brightness of the source, the redshift of the image, and the relative magnification. We

analyze the exact time delay and conclude that the EEH effect is not relevant.

It is worthwhile to stress the fact that the QED perturbations induced by the EEH metric on the shadow or on the bending angle, would be observable if one has accurate measurements of the mass of the black hole and distance to the observer. Presently, the improvements in observational capabilities and the combination of lensing measurements with other observational programs, such as orbital dynamic observations and x-ray heat maps (gas modeling), will provide further insights.

ACKNOWLEDGMENTS

[1] G. Mie, Grundlagen einer Theorie der Materie, Ann. Phys. (N.Y.) **342**, 511 (1912).

[2] M. Born, L. Infeld, and R. H. Fowler, Foundations of the new field theory, Proc. R. Soc. A **144**, 425 (1934).

[3] B. Hoffmann, Gravitational and electromagnetic mass in the Born-Infeld electrodynamics, Phys. Rev. **47**, 877 (1935).

[4] H. Salazar, A. García, and J. Plebański, Duality rotations and type D solutions to Einstein equations with nonlinear electromagnetic sources, J. Math. Phys. (N.Y.) **28**, 2171 (1987).

[5] J. F. Plebański, *Lectures on Nonlinear Electrodynamics* (Nordita, Copenhagen, 1970).

[6] A. García, H. Salazar, and J. Plebański, Type-D solutions of the Einstein and Born-Infeld nonlinear-electrodynamics equations, Il Nuovo Cimento B **84**, 65 (1984).

[7] E. Ayón-Beato and A. García, Regular Black Hole in General Relativity Coupled to Nonlinear Electrodynamics, Phys. Rev. Lett. **80**, 5056 (1998).

[8] W. Heisenberg and H. Euler, Folgerungen aus der Diracschen Theorie des Positrons, Z. Phys. **98**, 714 (1936).

[9] S. Weinberg, *The Quantum Theory of Fields* (Cambridge University Press, Cambridge, England, 1995), Vol. 2.

[10] Y. N. Obukhov and G. F. Rubilar, Fresnel analysis of wave propagation in nonlinear electrodynamics, Phys. Rev. D **66**, 024042 (2002).

[11] G. Boillat, Nonlinear electrodynamics: Lagrangians and equations of motion, J. Math. Phys. (N.Y.) **11**, 941 (1970).

[12] G. Brodin, M. Marklund, and L. Stenflo, Proposal for Detection of QED Vacuum Nonlinearities in Maxwell's Equations by the Use of Waveguides, Phys. Rev. Lett. **87**, 171801 (2001).

[13] R. Ruffini, Y.-B. Wu, and S.-S. Xue, Einstein-Euler-Heisenberg theory and charged black holes, Phys. Rev. D **88**, 085004 (2013).

[14] H. Yajima and T. Tamaki, Black hole solutions in Euler-Heisenberg theory, Phys. Rev. D **63**, 064007 (2001).

[15] D. Amaro and A. Macías, Geodesic structure of the Euler-Heisenberg static black hole, Phys. Rev. D **102**, 104054 (2020).

[16] The Event Horizon Telescope Collaboration *et al.*, First M87 event horizon telescope results. I. The shadow of the supermassive black hole, Astrophys. J. Lett. **875**, L1 (2019).

[17] V. Perlick, Exact gravitational lens equation in spherically symmetric and static spacetimes, Phys. Rev. D **69**, 064017 (2004).

[18] P. Schneider, J. Ehlers, and E. E. Falco, *Gravitational Lenses* (Springer-Verlag, New York, Berlin, Heidelberg, 1992).

[19] G. Meylan, P. Jetzer, P. North, P. Schneider, C. S. Kochanek, and J. Wambsganss, *Gravitational Lensing: Strong, Weak and Micro* (Springer, Berlin, Heidelberg, 2006).

[20] S. Dodelson, *Gravitational Lensing* (Cambridge University Press, Cambridge, England, 2017).

[21] K. S. Virbhadra and G. F. R. Ellis, Schwarzschild black hole lensing, Phys. Rev. D **62**, 084003 (2000).

[22] K. Virbhadra, D. Narasimha, and S. Chitre, Role of the scalar field in gravitational lensing, Astron. Astrophys. **337**, 1 (1998).

[23] S. Frittelli and E. T. Newman, Exact universal gravitational lensing equation, Phys. Rev. D **59**, 124001 (1999).

[24] S. Frittelli, T. P. Kling, and E. T. Newman, Spacetime perspective of Schwarzschild lensing, Phys. Rev. D **61**, 064021 (2000).

[25] J. Ehlers, S. Frittelli, and E. T. Newman, Gravitational lensing from a space-time perspective, in *Revisiting the Foundations of Relativistic Physics* (Springer, Netherlands, 2003), pp. 281–304.

[26] T. P. Kling and E. T. Newman, Null cones in Schwarzschild geometry, Phys. Rev. D **59**, 124002 (1999).

[27] E. F. Eiroa, Gravitational lensing by Einstein-Born-Infeld black holes, Phys. Rev. D **73**, 043002 (2006).

[28] W. Javed, J. Abbas, and A. Övgün, Deflection angle of photon from magnetized black hole and effect of nonlinear electrodynamics, Eur. Phys. J. C **79**, 694 (2019).

[29] Q.-M. Fu, L. Zhao, and Y.-X. Liu, Weak deflection angle by electrically and magnetically charged black holes from nonlinear electrodynamics, Phys. Rev. D **104**, 024033 (2021).

[30] X.-J. Gao, J.-M. Chen, H. Zhang, Y. Yin, and Y.-P. Hu, Investigating strong gravitational lensing with black hole metrics modified with an additional term, Phys. Lett. B **822**, 136683 (2021).

[31] M. Okyay and A. Övgün, Nonlinear electrodynamics effects on the black hole shadow, deflection angle, quasinormal modes and greybody factors, J. Cosmol. Astropart. Phys. 01 (2022) 009.

[32] G. Gibbons and C. A. R. Herdeiro, The Melvin universe in Born-Infeld theory and other theories of nonlinear electrodynamics, Classical Quantum Gravity **18**, 1677 (2001).

[33] J. L. Synge, The escape of photons from gravitationally intense stars, Mon. Not. R. Astron. Soc. **131**, 463 (1966).

[34] H. Goldstein, C. Poole, and J. Safko, *Classical Mechanics* (Addison Wesley, Reading, MA, 2002).

[35] S. Weinberg, *Gravitation and Cosmology: Principles and Applications of the General Theory of Relativity* (John Wiley and Sons, Inc., New York, 1972).

[36] E. F. Eiroa, G. E. Romero, and D. F. Torres, Reissner-Nordström black hole lensing, Phys. Rev. D **66**, 024010 (2002).

[37] X. Pang and J. Jia, Gravitational lensing of massive particles in Reissner–Nordström black hole spacetime, Classical Quantum Gravity **36**, 065012 (2019).